Magnetic properties of nanostructured ball-milled Fe and $Fe_{50}Co_{50}$ alloy

2006 J. Phys.: Condens. Matter 18 7257

(http://iopscience.iop.org/0953-8984/18/31/020)

INSTITUTE OF PHYSICS PUBLISHING JOURNAL OF PHYSICS: CONDENSED MATTER

J. Phys.: Condens. Matter **18** (2006) 7257–7272 doi:10.1088/0953-8984/18/31/020

Magnetic properties of nanostructured ball-milled Fe and $Fe_{50}Co_{50}$ alloy

S Azzaza[1], S Alleg[1], H Moumeni[1,2], A R Nemamcha[3], J L Rehspringer[4] and J M Greneche[5]

[1] Laboratoire de Magnétisme et Spectroscopie des Solides (LM2S), Département de Physique, Faculté des Sciences, Université de Annaba, BP 12 (23000) Annaba, Algeria
[2] Département de Physique, Faculté des Sciences et de l'Ingénierie, Université de Guelma, BP 401, (24000) Guelma, Algeria
[3] Laboratoire d'Analyse Industrielle et Génie des Matériaux, Faculté des Sciences et de l'Ingénierie, Université de Guelma, BP 401, (24000) Guelma, Algeria
[4] Groupe de Matériaux Inorganiques, Institut de Physique et de Chimie des Matériaux de Strasbourg, UMR 7504 CNRS-ULP, 23 rue de Loess, F-67034 Strasbourg cedex, France
[5] Laboratoire de Physique de l'Etat Condensé, UMR 6087 CNRS, Université du Maine, Faculté des Sciences, F-72085 Le Mans Cedex 9, France

Received 1 March 2006, in final form 27 June 2006
Published 21 July 2006
Online at stacks.iop.org/JPhysCM/18/7257

Abstract

Nanostructured Fe and $Fe_{50}Co_{50}$ powders were prepared by high-energy ball milling. Microstructural and magnetic properties changes with milling time were followed by x-ray diffraction, differential scanning calorimetry and vibrating sample magnetometry. The nonequilibrium microstructure originates from a grain size reduction to about 12 nm and the introduction of internal strain up to 1.5% (root-mean-square strain). The occurrence of disorder in the ball-milled powders is evidenced by the broad exothermic reaction during the heating of ball-milled samples, the variation of lattice parameters and the increase of the saturation magnetization during the first 3 h of milling for Fe and continuously for the $Fe_{50}Co_{50}$ powder mixture. According to both the reduction of Fe Curie temperature, T_c, and the increase of the phase transformation $T_{\alpha\rightarrow\gamma}$, the paramagnetic temperature domain of nanostructured bcc α-Fe is extended by about 50 °C. The $Fe_{50}Co_{50}$ nanostructured powder behaves as a soft ferromagnet with low values of both the coercive field and the squareness ratio M_r/M_s.

(Some figures in this article are in colour only in the electronic version)

1. Introduction

The high-energy ball-milling technique produces nanostructured materials by the structural disintegration of coarser-grained structure as a result of severe plastic deformation [1–4]. The nanostructured materials in powder form have the advantage of being able to be compacted to any configuration, being very interesting for the technological applications in which ribbon and wire shapes are not adequate. Because of the very fine grain size, a significant volume

of the microstructure in nanostructured materials is composed of interfaces, mainly grain boundaries. Consequently, nanostructured materials present a variety of properties that are significantly different from, and often an improvement on, those of their conventional coarse-grained polycrystalline counterparts [5, 6].

Iron–cobalt-based alloys present particularly interesting magnetic properties, with high Curie temperatures, the highest saturation magnetization (of all known magnetic alloys), high permeability, low losses, and also good mechanical properties such as high hardness [7, 8]. As for soft magnetic systems in general, the coercivity, H_c, of Fe–Co alloys depends strongly on the microstructure, whereas the saturation magnetization, M_s, is generally regarded as independent of the microstructure. In order to understand how the magnetic properties deteriorate as the grain size is decreased in the range 5–20 nm accessible by mechanical alloying (MA), particular emphasis was placed on making soft magnetic materials with the compositions of 25 to 50% Co in Fe [9–11]. This composition range has the highest moment per unit mass or volume of any magnetic material. Kuhrt *et al* have reported that MA seems to be unsuitable for producing soft magnetic nanostructured Fe–Co and Fe–Ni because of the amount of internal strain introduced into the material during the milling process, which is inevitably due to heavy plastic deformation and cannot be removed without the simultaneous occurrence of undesirable grain growth [11]. However, Fenineche *et al* have observed, for nanostructured Fe–Co, a regular and similar diminution of the coercivity and the crystallite size as a function of milling time [12], in good agreement with the theoretical predictions of the random-anisotropy model [13].

In previous Mössbauer studies on the mechanically alloyed $Fe_{50}Co_{50}$, the mixing process between elemental Fe and Co, at the atomic level, has been followed by the evolution of the hyperfine magnetic field distribution as a function of milling time [14, 15]. It has been observed that the initial peak at 33 T related to the unreacted α-Fe is progressively replaced by a broad distribution of higher hyperfine fields as the milling time increases. The obtained hyperfine magnetic field distribution, after 24 h of milling, exhibits a Gaussian shape centred at 35 T, attributed to the formation of a bcc Fe(Co) disordered solid solution.

In the present work, the nonequilibrium state of the microstructure, the correlation between the grain reduction and the magnetic properties of the milled powders such as the saturation magnetization, M_s, and the coercivity, H_c, in the nanostructured Fe and $Fe_{50}Co_{50}$ alloy, are discussed as a function of milling time.

2. Experimental procedure

Elemental iron (particle size $\sim$2 μm) and cobalt (particle size $\sim$45 μm) powders were milled in a planetary ball mill (Fritsch P7) under argon atmosphere using hardened steel containers and balls. The compositions of the initial powder mixture were Fe_{100} and $Fe_{50}Co_{50}$. The milling intensity was 400 rpm and the ball-to-powder weight ratio was 20:1. X-ray diffraction (XRD) investigations were performed on a D501 Siemens diffractometer using Cu Kα radiation ($\lambda = 0.154\,056$ nm). The properties of materials are mostly dependent on the grain size, therefore an accurate determination of such structural parameter is important. Hence, the x-ray diffraction patterns were analysed by using the Maud program based on both the Rietveld method and Fourier analysis [16]. The average grain size (the size of the coherently diffracting domain) was determined after the incorporation of the appropriate corrections for instrumental and strain effects. Differential scanning calorimetry (DSC) measurements were carried out using a universal Genessus 6000 differential scanning calorimeter within the temperature range 20–1000 °C at a continuous heating rate of 10 °C min^{-1}. The magnetic characterization of the ball-milled powders was carried out in a vibrating sample magnetometer (VSM) at 100 K, in an external field up to 17.4 kOe.

3. Results and discussion

3.1. Microstructure

In the $Fe_{50}Co_{50}$ powder mixture, Co is found to undergo an allotropic phase transformation from fcc to hcp form. This is evidenced, after 1 h of milling, by an increase of the hcp Co line intensities and the decrease of the fcc ones which disappear completely after 6 h. The fcc Co phase is metastable at room temperature, and becomes unstable when an external mechanical or thermal energy is introduced [17]. Hence, the fcc Co phase transforms to the hcp Co phase, at the early stage of milling, owing to the accumulation of structure defects and the increase of the energy stored in the materials during the milling process. Both the repeated fracturing and welding of powder particles increase the area of contact between the reactant powder particles due to a reduction in particle size and this allows fresh surfaces to come into contact repeatedly. This permits the reaction to proceed without the necessity for diffusion through the produced layer. As a consequence, the reactions that normally require high temperature occur at lower temperature during MA without any external heating treatment. Also, the high defect densities induced during the milling accelerate the diffusion process. Alternatively, the particle refinement and the subsequent reduction in diffusion distances can at least reduce the reaction temperature significantly, even they do not occur at room temperature. After more than 12 h of milling, the disappearance of the hcp Co diffraction peaks and therefore the diffusion of Co into the Fe matrix leads to the formation, after 24 h of milling, of a disordered bcc Fe(Co) solid solution with a mean lattice parameter $a = 0.2861(5)$ nm, larger than that of the coarse-grained FeCo ($a = 0.2825(5)$ nm). The best Rietveld refinement of the XRD patterns of ball-milled pure Fe and $Fe_{50}Co_{50}$ powder mixture for 40 h is shown in figures 1(a) and (b), respectively, and the fitting results are summarized in table 1.

The grain size decreases significantly with milling up to 9 h, becomes about 12(2) nm for both Fe and $Fe_{50}Co_{50}$ powder mixture and remains rather milling time independent. Simultaneously, the microstrains increase owing to the heavy plastic deformation to about 1.2(2) and 1.6(2)% (rms strain) for Fe and $Fe_{50}Co_{50}$ powders, respectively. Figure 2 shows a double logarithmic plot of measured grain size as a function of milling time for Fe (figure 2(a)) and $Fe_{50}Co_{50}$ powders (figure 2(b)). According to the alloying process (crystallite size refinement), the grain size plot exhibits a two-stage behaviour. A linear fit gives: (i) a slope of -0.65 for short milling times and of -0.20 for extended milling times, in the case of Fe; and (ii) slopes of -0.85 and -0.03, respectively, for the first (short milling times) and the second (extended milling times) regimes, for the $Fe_{50}Co_{50}$ powder mixture. According to the model proposed by Li *et al*, which describes the evolution of nanostructured grain size during mechanical deformation [18], the critical grain size achievable by ball milling is defined by the crossing point between the two regimes with different slope. Thus, critical grain sizes are of 13.8 and 15 nm for Fe and $Fe_{50}Co_{50}$ powders, respectively. By using different types of mills with different milling intensity and temperature to prepare nanostructured Fe powders, Börner *et al* have shown that the proposed model by Li *et al* is not valid for all materials. Indeed, they obtained a two-regime behaviour for the grain refinement by using a Spex mill, with slopes of -0.41 and -0.08, respectively, for short and extended milling times. However, the grain sizes show only a simple linear relation with slopes of -0.265 and -0.615 by using a Retsch MM2 shaker mill and a Misuni vibration mill, respectively. The calculated critical grain size value was 19 nm [19].

3.2. Thermal stability

The thermal stability of nanostructured Fe powders is followed by DSC scans, as shown in figure 3. The broad exothermic reaction, which consists of two or three overlapping exothermic

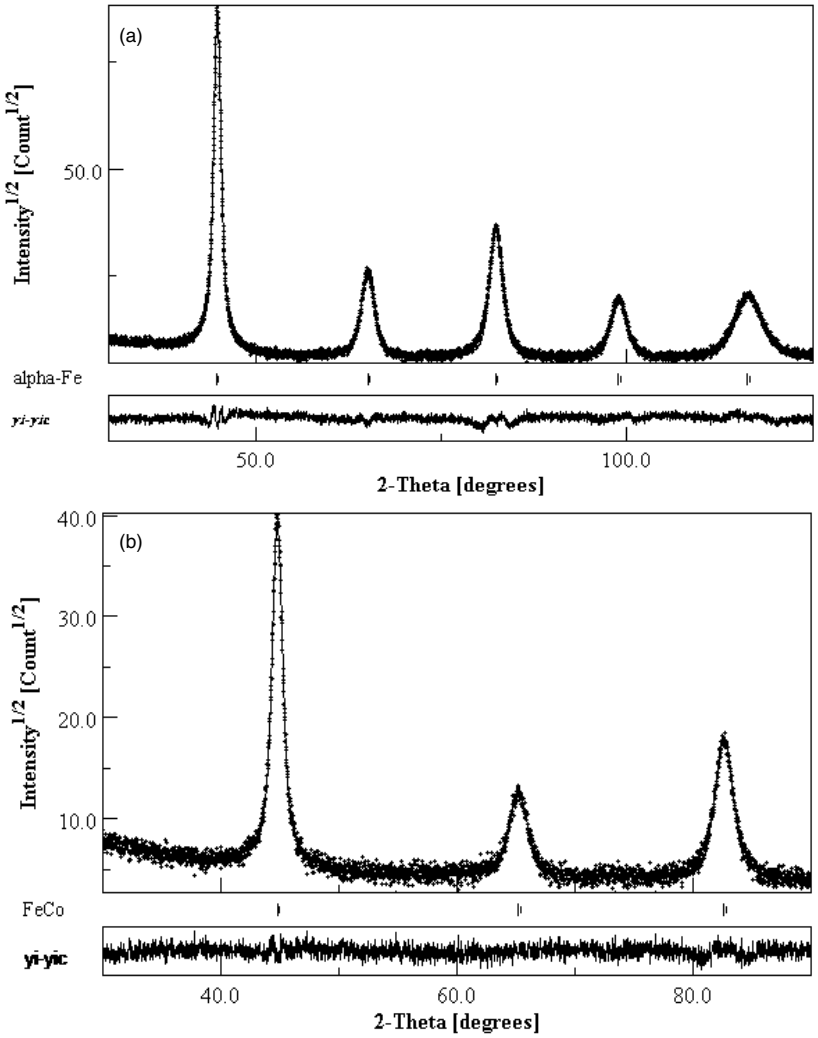

Figure 1. XRD patterns of pure Fe (a) and $Fe_{50}Co_{50}$ powder mixture (b) milled for 40 h. The difference (yi – yic) between experimental (dots) and calculated (full line) patterns is given below.

Table 1. Lattice parameter, a, average grain size, $\langle d \rangle$, microstrain, $\langle \sigma^2 \rangle^{1/2}$, and goodness of fit, χ, of pure Fe and $Fe_{50}Co_{50}$ powder mixture milled for 40 h.

	a (nm)	$\langle d \rangle$ (nm)	$\langle \sigma^2 \rangle^{1/2}$	χ
Fe	0.2874(5)	12(2)	1.20(5)	1.18(5)
$Fe_{50}Co_{50}$ powder mixture	0.2861(5)	12(2)	1.60(8)	1.12(5)

peaks, occurs for all samples and spreads over the temperature range 100–600 °C. This behaviour, which is very similar to that observed for other crystalline metals and nanostructured materials [20–22], originates from recovery, strain relaxation and grain growth. Since the transition heats evolving in the atomic reordering and in the grain growth are comparable in value [20], both atomic disorder and nanocrystallite boundaries are thus major sources of

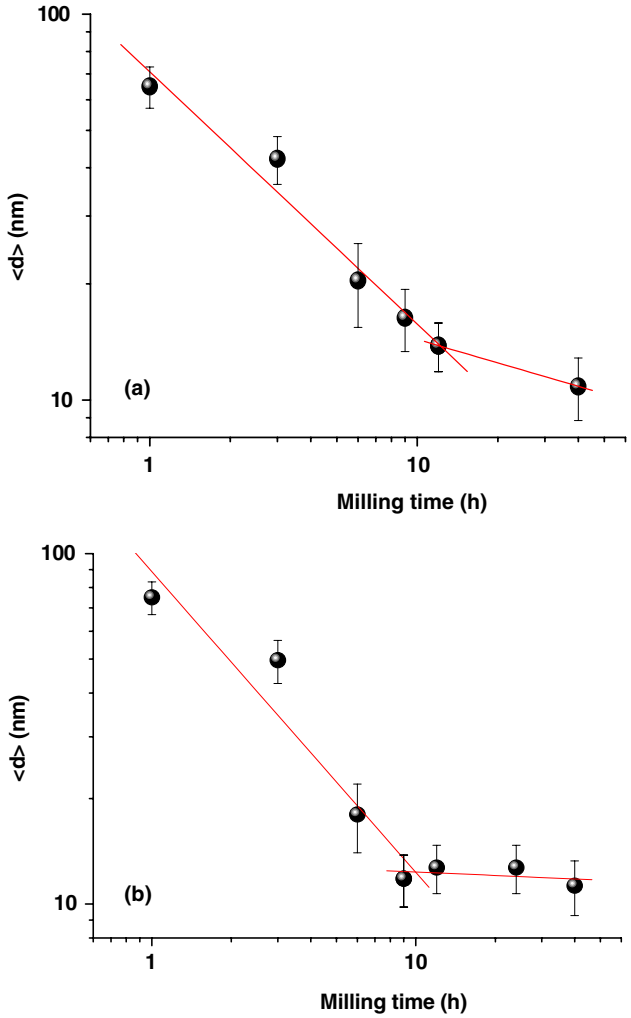

Figure 2. Double logarithmic plot of the grain size as a function of milling time for pure Fe (a) and $Fe_{50}Co_{50}$ powder mixture (b).

mechanical energy storage. The decrease of the exothermic peak temperature with increasing milling time indicates a decrease of crystallite size.

The Curie temperature, T_c, of the ball-milled Fe powders is deduced from the DSC scans (first endothermic peak) and plotted versus milling time in figure 4. One observes that the Curie temperature decreases rapidly between 3 and 12 h and slightly upon further milling time. After 40 h of milling, the obtained value of about 761 °C is slightly lower than that of bulk iron ($T_c = 770$ °C). The decrease of Curie temperature might be due to the grain size decreasing. In fact, if the grain sizes are small enough, the structural distortions associated with the surfaces or interfaces can lower the Curie temperature. The structural distortions can be confirmed by the Fe lattice parameter increasing with the milling time. It has been reported on far-from-equilibrium nanostructured metals that interfaces present a reduced atomic coordination and a wide distribution of interatomic spacings compared to the crystals, and consequently, the atomic arrangement at the grain boundary may be considered close to the amorphous

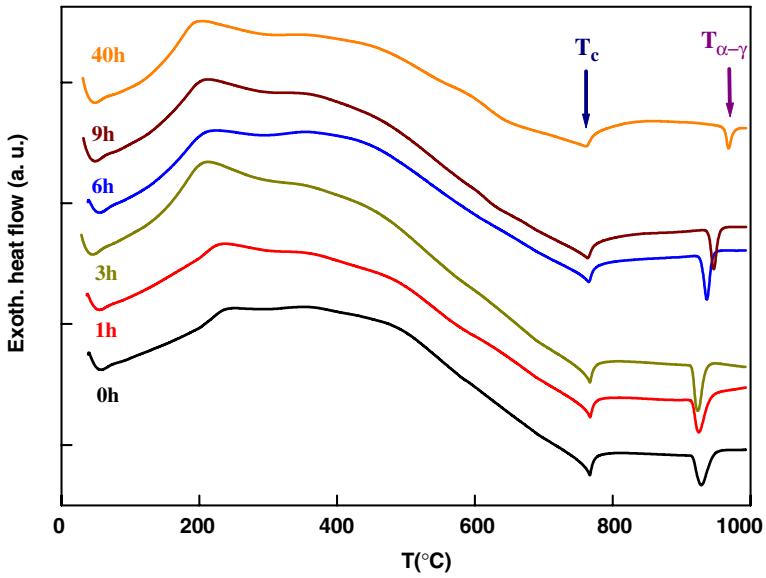

Figure 3. DSC traces of milled pure Fe for various times (heating rate 10 °C min^{-1}).

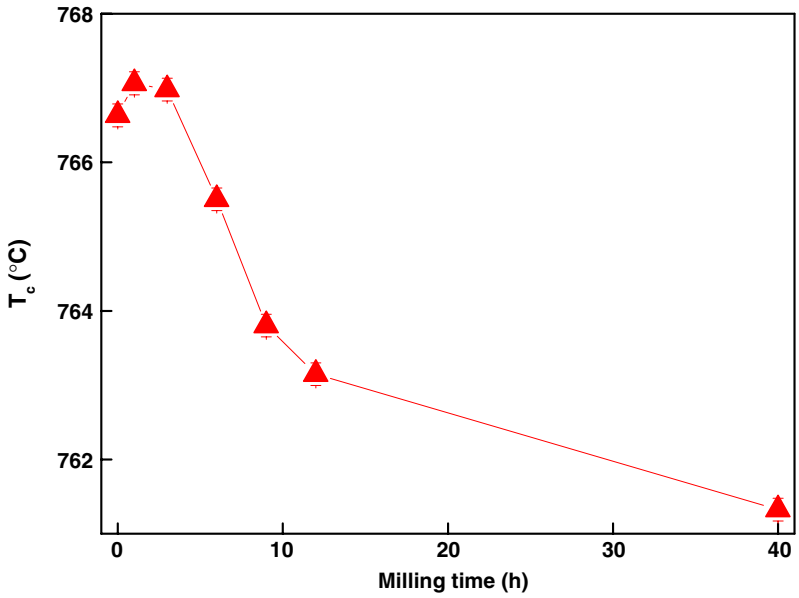

Figure 4. Curie temperature variation of milled pure Fe as a function of milling time.

configuration and should therefore alter the Curie temperature [23]. For most observations in the literature, the Curie temperature does not deviate strongly from that of the bulk materials. Host *et al* have reported a T_c value of 1093 °C for carbon arc produced Co[C] nanoparticles, in good agreement with the 1115 °C value for bulk Co [24]. The Curie temperature of 10 nm Gd is decreased about 10 K from that of coarse-grained Gd while the magnetic transition is broader [25].

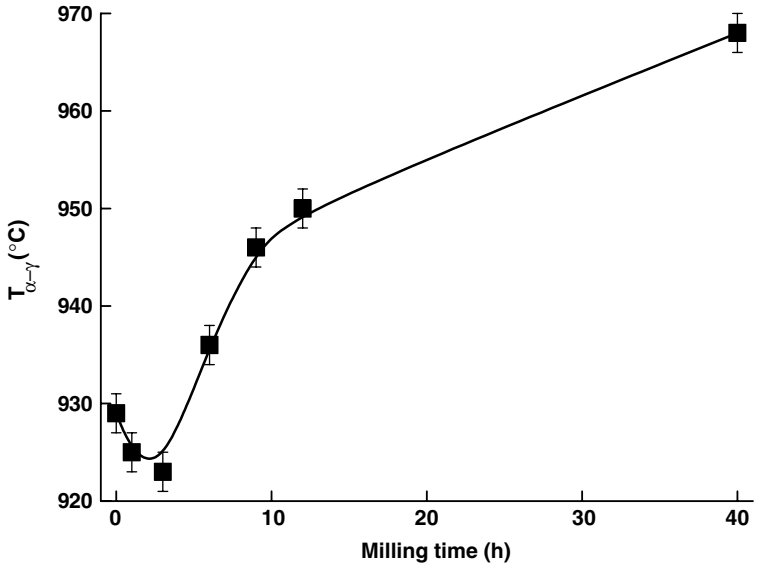

Figure 5. The $\alpha \rightarrow \gamma$-Fe phase transformation temperature versus milling time.

The volume expansion of the interfacial components in the nanostructured Fe can be evidenced by Mössbauer experiments [14, 15]. The best fit of the room-temperature Mössbauer spectrum of the ball-milled Fe for 40 h was obtained with three components consistent with the existence of two states for the Fe atoms. For the first state, the component of the hyperfine magnetic field $H_1 = 33.1(2)$ T is similar to that of bulk Fe, while, for the second state, there are observed two components which exhibit increased and reduced values of the hyperfine magnetic field close to $H_2 = 34.1(2)$ T and $H_3 = 31.2(2)$ T, respectively, compared with that of the first state (33.1 T). According to the Bethe–Slater curve, an increase in the near-neighbour distance would, in the case of Fe, lead to an increased value in the magnetic moment per atom and hence an increased magnetic hyperfine field [26, 27]. Hence, the hyperfine magnetic field $H_2 = 34.1(2)$ T in the second state of Fe atoms might be due to a wide distribution of interatomic spacings and can thus explain the reduction of nanostructured Fe Curie temperature.

The evolution of the bcc α- to fcc γ-Fe phase transformation temperature (second endothermic peak), $T_{\alpha\rightarrow\gamma}$, is presented as a function of milling time (figure 5). Noticeable is the monotonic increase of the $\alpha \rightarrow \gamma$ transformation temperature after more than the first 3 h of milling; it reaches a value of about 970 °C after 40 h. According to the variations of both the Curie temperature and the $\alpha \rightarrow \gamma$ Fe phase transformation temperature ($T_{\alpha\rightarrow\gamma}$), it is obvious that the paramagnetic nanostructured bcc α-Fe domain is extended by about 50 °C at the expense of both magnetic bcc α-Fe and nonmagnetic fcc γ-Fe as compared to coarse-grained bcc α-Fe.

For the mechanically alloyed $Fe_{50}Co_{50}$ powders, typical DSC scans are given in figure 6 as a function of milling time. The transition shape, the transition heat and the peak temperature are sensitive to the milling time. The nonequilibrium state is revealed by the broad exothermic reaction for all of the samples, in the temperature range 100–600 °C, which is consistent with the energy release during heating due to recovery, grain growth, relaxation processes within the grain boundaries. As a result of the cold work during the MA process, the major energy contribution is stored in the form of grain boundaries and related strains within the nanostructured grains which are induced through grain boundary stresses [28]. It has been

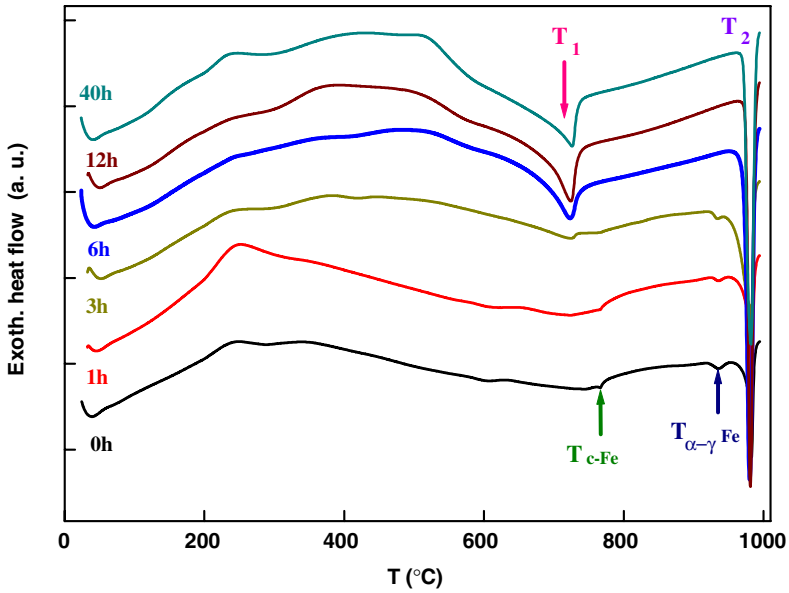

Figure 6. DSC traces of mechanically alloyed $Fe_{50}Co_{50}$ (heating rate 10 °C min^{-1}).

shown that the final energies stored during MA largely exceed those resulting from conventional cold working of metals and alloys, since they can reach values typical for crystallization enthalpies of metallic glasses corresponding to about 40% of the heat of fusion ΔH_f [28]. Figure 6 exhibits in addition to the broad exothermic peak, the presence of 4, 3 or 2 endothermic peaks depending on the milling stage. Thus, up to 1 h of milling, the endothermic peaks related to the Curie temperature and to the allotropic bcc → fcc phase transformation of the elemental Fe are observed together with a strong peak at a temperature of 980 °C attributed to the $\alpha \rightarrow \gamma$ FeCo phase transition. Thereafter, the DSC curve of the milled $Fe_{50}Co_{50}$ powders for 3 h reveals the existence of a new small endothermic peak at $T_1 = 725$ °C, corresponding to the $\alpha \rightarrow \alpha'$ disorder–order phase transformation of the FeCo solid solution and indicating, thus, the beginning of the atomic mixing between elemental Fe and Co powders. Thereby, beyond 6 h of milling the DSC traces show only two endothermic peaks related to the $\alpha \rightarrow \alpha'$ disorder–order and to $\alpha \rightarrow \gamma$FeCo, T_2, phase transformations.

The $\alpha \rightarrow \alpha'$ disorder–order phase transformation temperature of the Fe(Co) solid solution, which is nearly constant (∼724 °C) during the milling process (figure 7), is comparable to that of bulk Fe–Co alloys. It is commonly accepted that Fe–Co undergoes an ordering transition at around 730 °C, where the bcc structure takes the ordered α'-CsCl (B2)-type structure [29]. This result confirms the disordered bcc structure of the nanostructured FeCo powders. Similar behaviour has been observed in the DTA data of the carbon-coated $Fe_{0.5}Co_{0.5}$ alloy nanoparticles produced using an RF plasma torch [10]. The ordering effect in the FeCo nanocrystals, at about ∼730 °C, has been also revealed by the changes in the magnetization upon heating and the temperature variation of the coercivity on heating and cooling [10].

The variation of the $\alpha \rightarrow \gamma$ phase transformation temperature in the nanostructured $Fe_{50}Co_{50}$ powders is plotted against milling time in figure 8. Noticeable is the nearly constant temperature value of 982 °C, which is milling time independent. The lower resistivity of $Fe_{50}Co_{50}$ compared to that of pure Fe at 300 K [30] and the higher Curie temperature of $Fe_{50}Co_{50}$ suggests that there is less scattering of the conduction electrons by the magnetic

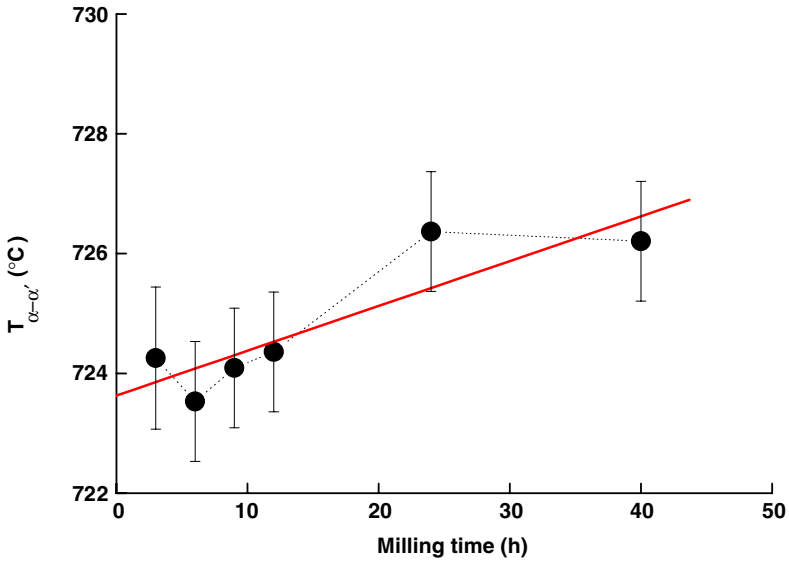

Figure 7. The $\alpha \rightarrow \alpha'$ disorder–order phase transformation temperature of the $Fe_{50}Co_{50}$ powder mixture versus milling time.

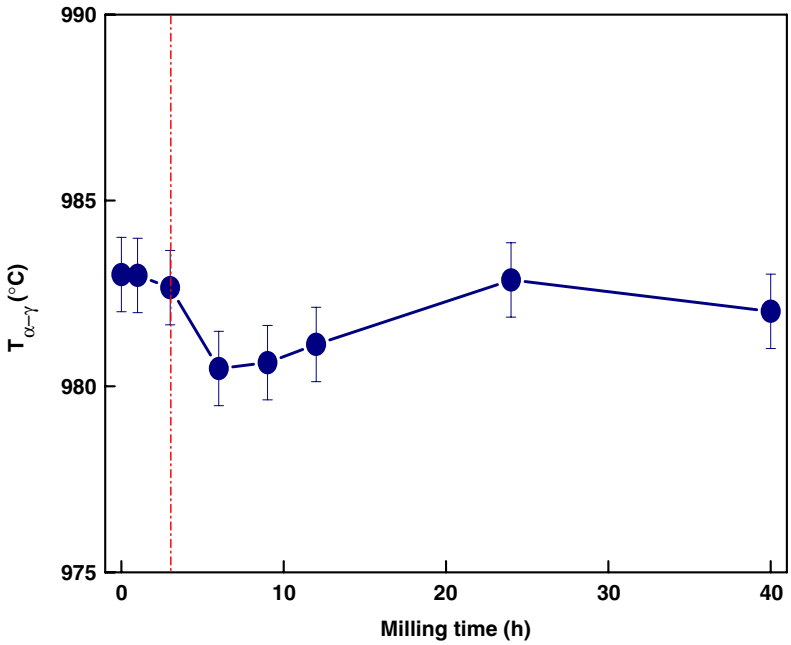

Figure 8. The $\alpha \rightarrow \gamma$ FeCo phase transformation temperature against milling time.

excitations. Thus, the Curie temperature cannot be unambiguously observed because there is a phase transformation from the bcc to the fcc form at 985 °C according to the Fe–Co phase diagram [29]. In fact, for Co concentrations more than 17%, the phase transformation to the nonmagnetic γ phase occurs while the α phase is still ferromagnetic, leading to the Curie

temperatures for the α phase which are greater than the $\alpha \rightarrow \gamma$ transition temperature. The $\alpha \rightarrow \gamma$ phase transformation temperature (982 °C) is rather higher than that obtained in the carbon-coated $Fe_{0.5}Co_{0.5}$ alloy nanoparticles, $T_{\alpha\rightarrow\gamma} \sim 950$ °C [10].

3.3. Magnetic measurements

The changes in the magnetic properties of nanoscale ferromagnetic materials usually originate from the microstructure and are attributed to the large fraction of atoms associated with the grain boundaries/interfaces, linking single-domain crystalline grains.

Figure 9 illustrates the milling time dependence of the hysteresis loops, at 100 K, of the ball-milled Fe (figure 9(a)) and $Fe_{50}Co_{50}$ powders (figure 9(b)). These sigmoidal hysteresis cycles are usually observed in nanostructured samples with small magnetic domains. This is due to the presence of structural distortions inside grains. The small hysteresis losses are properties generally desired in soft magnetic materials.

Figure 10 presents the dependence of coercivity H_c with grain size for the ball-milled Fe. The increase of the coercivity during the first 3 h of milling (up to 35 Oe), can be related to the plastic deformation effect and consequently to the introduction of internal strain and of different types of defect, which serve as pinning sites for the magnetic domain wall movement. It has been observed at this stage of milling that the Fe powder particles are flattened by compressive forces [14]. After more than 6 h of milling, H_c decreases with decreasing grain size up to 24 Oe and then levels off. The reduction of the coercivity, which can be attributed to the deviation of interatomic spacings in the interfacial regions as compared with the crystalline component, is consistent with the predictions of the random anisotropy model. For grain sizes comparable with the magnetic exchange length, $L = (A/K)^{1/2}$, where A is the exchange stiffness and K is the magnetocrystalline anisotropy, there is a plateau on the H_c versus d curve; in addition, for smaller grain sizes a sharp decrease ($H_c \sim d^6$) is expected because of the drastic decrease of the effective K determined by averaging over the grains above which the domains are extended [31]. The observed drop on the curve of H_c versus grain size is the first experimental verification of the model for ball-milled elemental Fe powders. The soft magnetic behaviour of as-milled pure iron powder has recently been reported [32]. It is observed that the coercive field of about 20 Oe for crystalline grain size of around 11 nm does not change with the milling time up to 48 h.

Figure 11 presents the variation of the coercivity and of the grain size of the ball-milled $Fe_{50}Co_{50}$ powder mixture as a function of milling time. It can be seen that the maximum value of H_c is observed after 1 h of milling and H_c decreases with decreasing grain size, up to 9 h, then increases slightly for longer milling times, while the grain size levels off. The H_c enhancement for short milling times can be a consequence of the transformation from fcc to hcp Co, since, in general, hcp structures are known to have larger magnetocrystalline anisotropy than fcc ones [33]. The reduction of grain size resulted in the decrease of the coercivity, in good agreement with the theoretical predictions of the random-anisotropy model. This result differs from that obtained by Kuhrt *et al* [11]. The authors have reported that the coercivity of the MA Fe–Co powders is milling time independent but pronounced composition dependence was observed similar to that of the Slater–Pauling curve established for bulk alloys.

Figure 12 shows the saturation magnetization versus milling time for the ball-milled Fe. The magnetization increases in the early stage of milling, reaches a maximum after 3 h, decreases rapidly up to 9 h, then levels off on further milling. The increase of the saturation magnetization indicates the introduction of atomic disorder by the milling process during the first 3 h of milling. The heavy plastic deformation of the ductile Fe powder particles which is followed by repeated fracturing and cold welding leads to the particle size

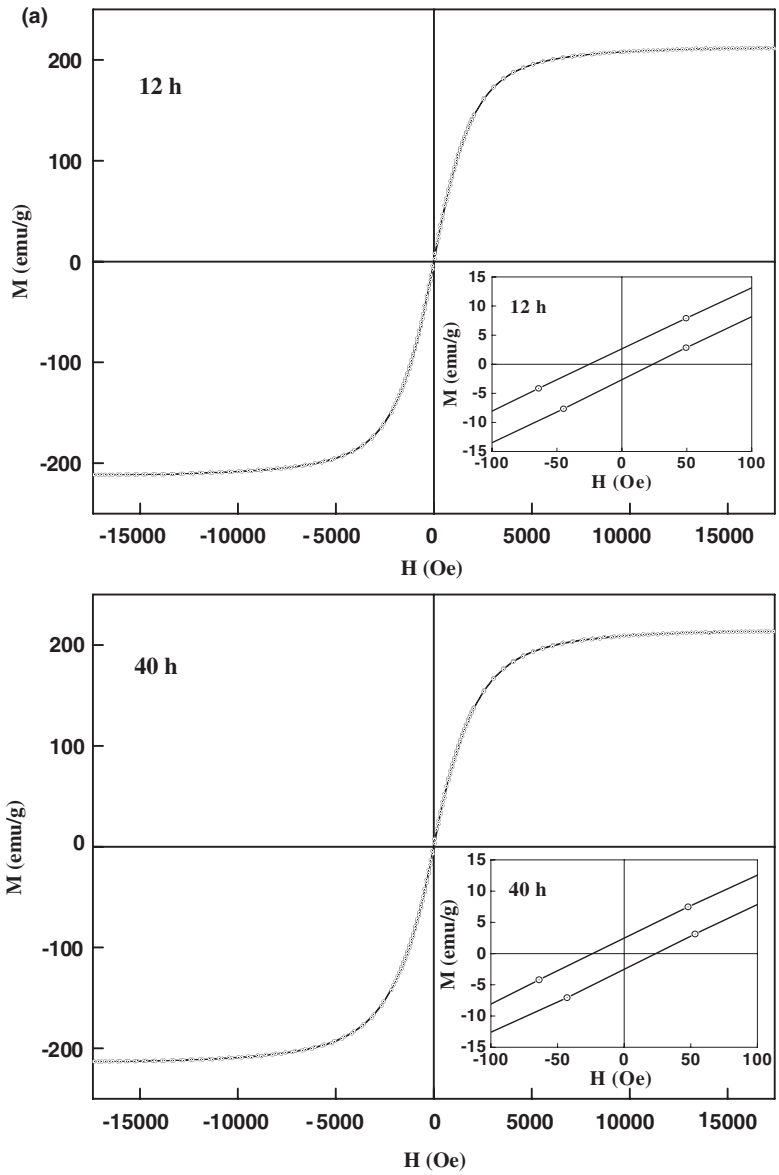

Figure 9. Typical hysteresis loops dependence on milling time, at $T = 100$ K, of Fe (a) and $Fe_{50}Co_{50}$ powder mixture (b). The inset is an enlargement of low-field region.

refinement and the introduction of high density of defects, particularly dislocations. Such defects cause a 0.5% volume expansion and consequently changes in geometry of the atomic arrangement and interatomic distances (which have an effect on the exchange interaction and hence the mode of spin alignment). Since the magnetization is created by domain wall movement and spin rotation, it can thus be affected by the induced structural defects. The increase of lattice parameter provides additional evidence for the occurrence of atomic disorder during milling (figure 12). It has been reported that there is a good correlation between the saturation magnetization and the lattice parameter (increase of both the lattice parameters and

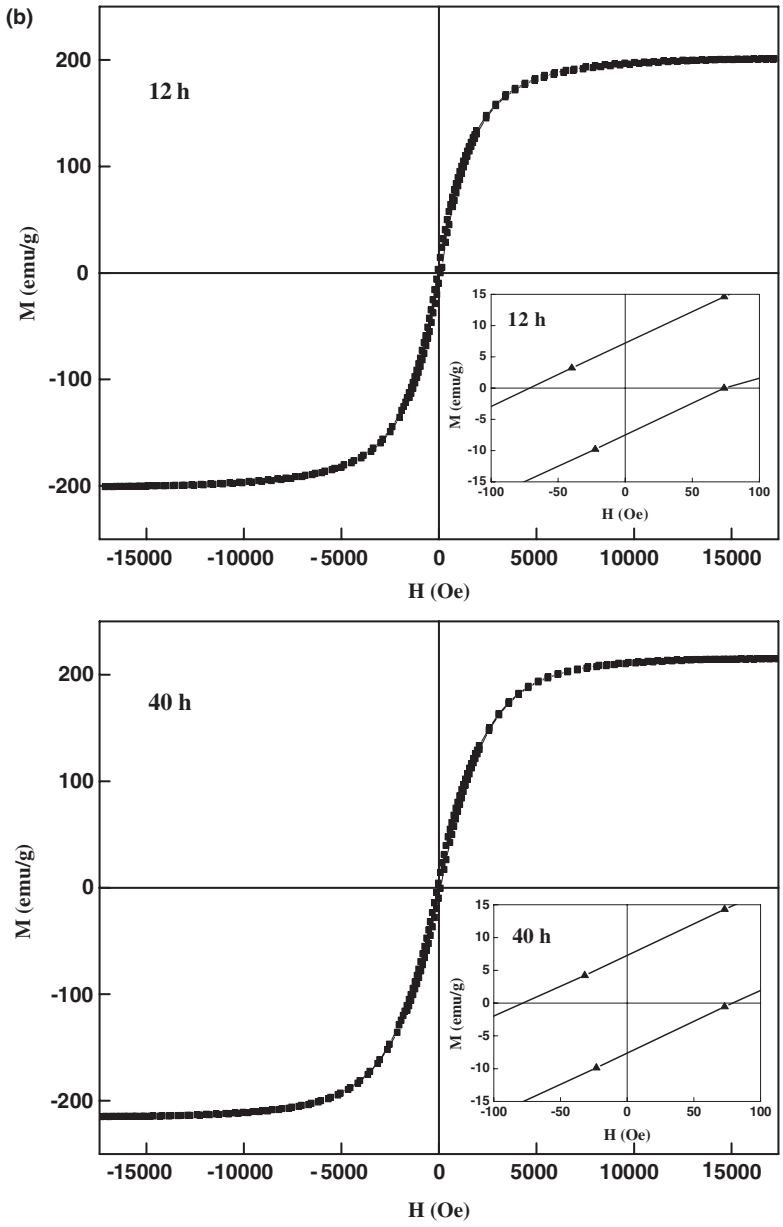

Figure 9. (Continued.)

the saturation magnetization) in the Fe–Al alloys, which suggests that the observed magnetic transition may be partially related to the changes in the density of states at the Fermi level [34]. Magnetization decreasing with grain size refinement after more than 3 h of milling may be due to the influence of grain boundary atoms, whose arrangement is quite different from that within the grains and results in lower magnetization. The obtained M_s value after 40 h of milling (213 emu g^{-1}) is comparable to that found by Brüning *et al* [9]. The authors have found that the M_s of the milled Fe powders in a planetary ball mill P5 decreased up to 209 emu g^{-1} after

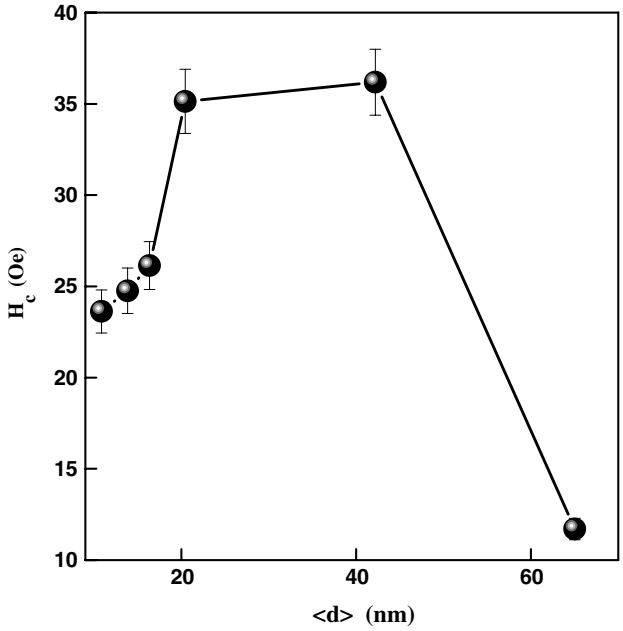

Figure 10. Dependence of the coercivity, H_c, with grain size in ball-milled pure Fe.

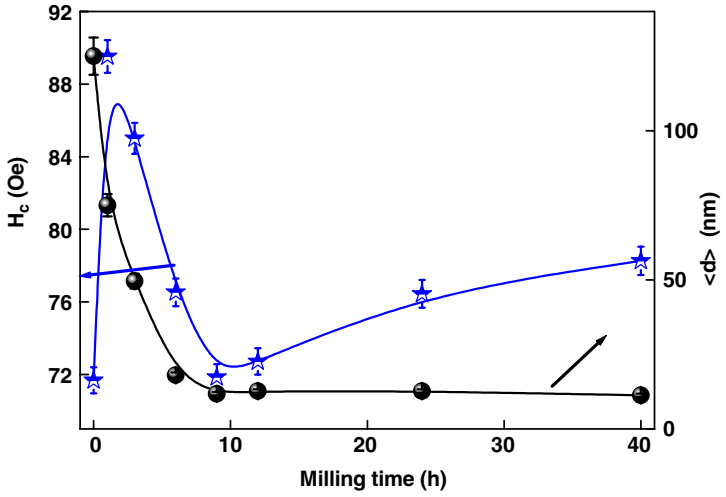

Figure 11. Coercive field H_c and the grain size variations of the ball-milled $Fe_{50}Co_{50}$ powder mixture as a function of milling time.

212 h of milling [9]. However, the M_s of 6 nm Fe was reported to be 130 emu g^{-1} compared to 220 emu g^{-1} for normal polycrystalline powder [35]. This reduction was attributed to the deviation of interatomic spacings in the interfacial regions as compared with the crystalline component.

The progress of alloying reaction between elemental Fe and Co powders during the MA process can be monitored by means of saturation magnetization changes (figure 13). The magnetization increases monotonically with the milling time and saturates after 24 h

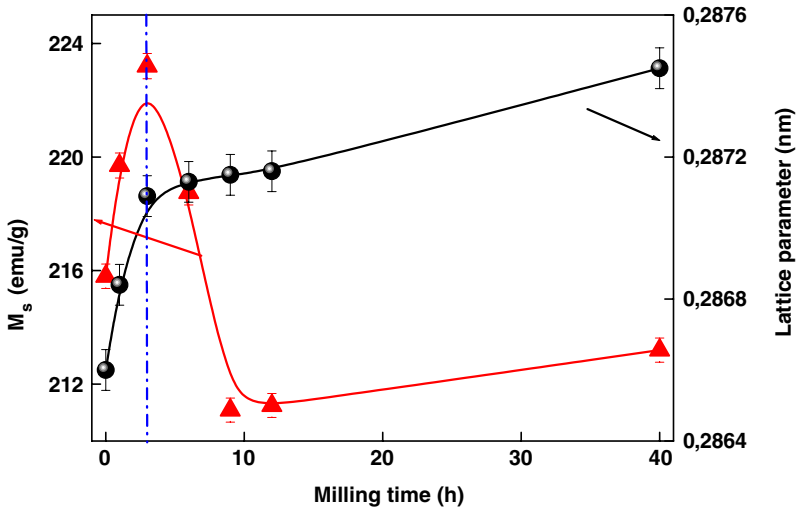

Figure 12. Saturation magnetization, M_s, and lattice parameter changes of pure Fe as a function of milling time.

($M_s = 215$ emu g^{-1}). The increase of the magnetization is found to be linked to the grain size reduction to about 12 nm. Each grain may be considered as being a single magnetic domain eliminating the influence from magnetic walls [36]. For much smaller grains, the ferromagnetic exchange interaction predominates and prevents the magnetic moments from alignment parallel to the easy axis of each individual grain. This results in a considerable reduction of the effective anisotropy by averaging over several grains, presuming that the randomly oriented grains are perfectly coupled via the exchange interaction (random anisotropy model). Different magnetization values were reported for the $Fe_{50}Co_{50}$ powders. Thus, M_s-values of 210 emu g^{-1} [11] and 232 emu g^{-1} [9] were obtained after 60 and 64 h of milling, respectively, in a planetary ball mill, while the largest magnetization of about 250 emu g^{-1} was found for the carbon-coated transition metal $Fe_{0.5}Co_{0.5}$[C] nanoparticles [37].

The continuous increase of the magnetization during the milling process is accompanied by a decrease of the lattice parameter of the $Fe_{50}Co_{50}$ powder mixture (figure 13). The decrease of the lattice parameter may be due to the so-called triple-defect disorder [38]. A triple defect consists of one anti-site Co atom combined with two vacancies on the Co sublattice. Thus, the decrease of the lattice parameter can be understood from the point of view of relaxation around the numerous vacancies. Anti-site disorder can be introduced since no vacant lattice sites are available in the structure. This means that, during milling, Co and Fe atoms will exchange position; such an exchange will lead to a variation of the Co atom neighbouring (each Co atom is surrounded by Co atoms as nearest neighbours). Thus, the clustering is favoured with more and more Co atoms surrounding a Co atom. Such a Co-rich cluster will bear a larger magnetic moment because of an increasing probability of Co–Co exchange interactions. The number of Co-rich clusters will gradually increase with increasing milling time. This will lead to an increase of the average magnetization which clearly show a significant change of magnetic moment after ball milling due to the change of the nearest-neighbour configuration of the magnetic elements Fe and Co. This might be supported by Mössbauer spectrometry measurements [15]. Indeed, the existence of one component with an hyperfine field below 33.0 T attributed to dilute Fe solutes in a Co matrix up to 9 h of milling and another component with $H = 33.0$ T and IS $= 0.07$ mm s^{-1} has been reported.

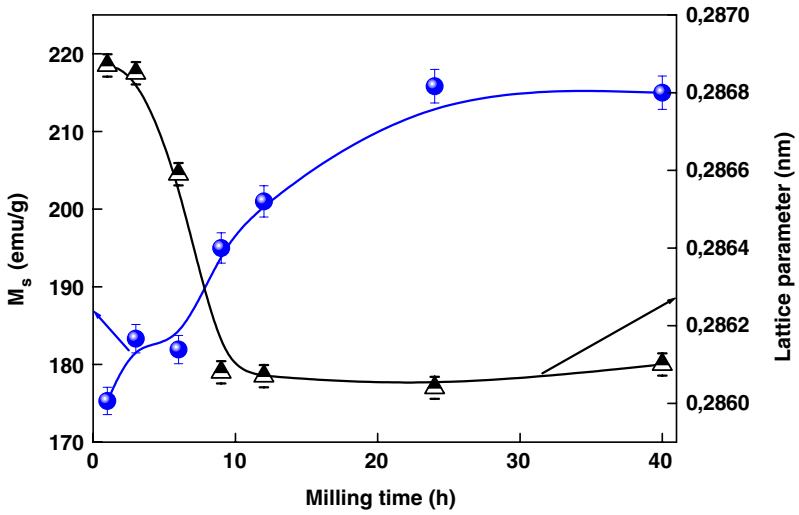

Figure 13. Saturation magnetization, M_s, and lattice parameter changes of $Fe_{50}Co_{50}$ powder mixture as a function of milling time.

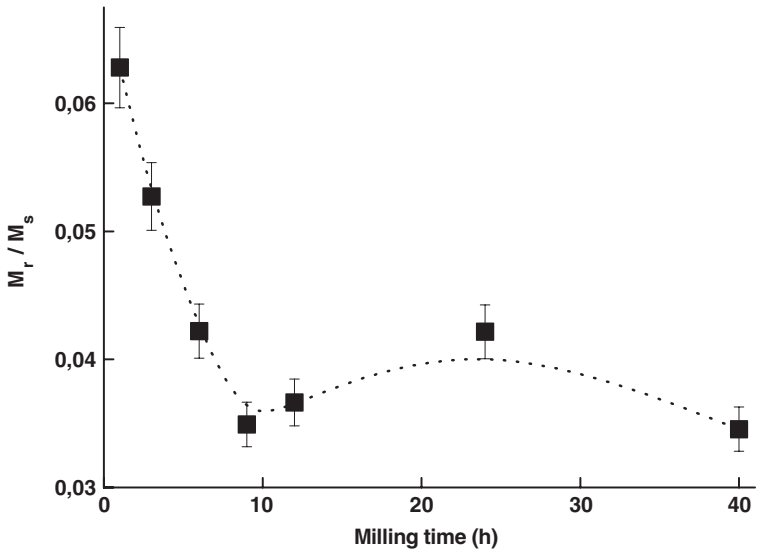

Figure 14. The remanence-to-saturation ratio M_r/M_s as a function of milling time for the $Fe_{50}Co_{50}$ powder mixture.

The remanence-to-saturation ratio, M_r/M_s, which is an other important magnetic parameter in determining the magnetic energy, is plotted against milling time in figure 14. The magnetic squareness ratio decreases rapidly with increasing milling time up to 9 h, and remains nearly constant with further milling. Such lower values of M_r/M_s indicate that the small magnetic particles are typically single domains. The M_r/M_s ratio value is comparable to that obtained for 90%Co–10%Ni alloy after 72 h of milling [12].

4. Conclusion

Soft magnetic nanostructured Fe and $Fe_{50}Co_{50}$ powders were obtained by MA in a high-energy planetary ball mill P7 with critical grain sizes of about 14 and 15 nm, respectively. In the nanostructured Fe powders, the bcc α-Fe paramagnetic temperature domain is extended at the expense of both magnetic bcc α-Fe and nonmagnetic fcc γ-Fe as the milling process progresses. The coercivity, H_c, followed the predictions of the random-anisotropy model and the saturation magnetization is grain size dependent.

For the $Fe_{50}Co_{50}$ powder mixture, the solid solution is formed after 24 h of milling with a bcc structure and a lattice parameter of about 0.2861 nm. The $\alpha \rightarrow \alpha'$ disorder $\rightarrow$ order and $\alpha \rightarrow \gamma$ phase transformations are observed at about 724 and 982 °C, respectively. The coercivity, H_c, remanence-to-saturation ratio, M_r/M_s, and grain size exhibit similar reduction with increasing milling time. A slight increase occurred after 24 h of milling for both H_c and M_r/M_s ratio. The saturation magnetization is practically independent of the grain size and its increase indicates the introduction of atomic disorder by ball milling.

References

[1] Suryanarayana C 2000 *Prog. Mater. Sci.* **46** 1
[2] Koch C C 1993 *Nanostruct. Mater.* **2** 109
Koch C C 1997 *Nanostruct. Mater.* **9** 13
[3] Bentayeb F Z, Alleg S, Bouzabata B and Greneche J M 2005 *J. Magn. Magn. Mater.* **288** 282
[4] Bensebaa N, Alleg S and Greneche J M 2005 *J. Alloys Compounds* **393** 194
[5] Gleiter H 1995 *Nanostruct. Mater.* **6** 3
[6] Birringer R, Gleiter H, Klein H P and Marquardt P 1984 *Phys. Lett.* A **102** 365
[7] Pfeifer F and Radeloff C 1980 *J. Magn. Magn. Mater.* **19** 190
[8] Rajkovic M and Buckley R A 1981 *Met. Sci.* **15** 21
[9] Brüning R, Samwer K, Kuhrt C and Schultz L 1992 *J. Appl. Phys.* **72** 2978
[10] Turgut Z, Huang M Q, Gallagher K and McHenry M E 1997 *J. Appl. Phys.* **81** 4039
[11] Kuhrt C and Schultz L 1992 *J. Appl. Phys.* **71** 1896
[12] Fenineche N E, El Kedim O and Gaffet E 2000 *J. Met. Nanocryst. Mater.* **7** 41
[13] Löffler J and Weissmüller J 1995 *Phys. Rev.* B **52** 7076
[14] Moumeni H 2005 *PhD Thesis* University of Annaba, Algeria
[15] Moumeni H, Alleg S and Greneche J M 2005 *J. Alloys Compounds* **386** 12
[16] Lutterotti L 2000 *MAUD CPD Newsletter (IUCr)* **24**
[17] Huang J Y, Wu Y K, Ye H Q and Lu K 1995 *Nanostruct. Mater.* **6** 723
[18] Li S, Wang K, Sun L and Wang Z 1992 *Scr. Metall. Mater.* **27** 437
[19] Börner I and Eckert J 1997 *Mater. Sci. Eng.* A **226–228** 541
[20] Zhou G F and Bakker H 1994 *J. Phys.: Condens. Matter* **6** 4043
[21] Yavari A R 1993 *Acta Metall. Mater.* **41** 1391
[22] Zhou G F and Bakker H 1996 *Scr. Mater.* **34** 29
[23] Lu K and Sun N X 1997 *Phil. Mag. Lett.* **75** 389
[24] Host J J, Teng M H, Elliot B R, Hwang J H, Mason T O and Johnson D L 1997 *J. Mater. Res.* **12** 1268
[25] Krill C E, Merzoug F, Krauss W and Birringer R 1997 *Nanostruct. Mater.* **9** 455
[26] Gonser U 1991 *Hyperfine Interact.* **68** 71
[27] Herr U, Jing J, Birringer R, Gonser U and Gleiter H 1987 *Appl. Phys. Lett.* **50** 472
[28] Fecht H J 1994 *Nanophase Materials* ed G C Hadjipanayis and R W Siegel (Dordrecht: Kluwer) p 125
[29] Massalski T 1990 *Binary Alloy Phase Diagrams* (Materials Park, OH: ASM International)
[30] Persiano A I C and Rawlings R D 1991 *J. Mater. Sci.* **26** 4026
[31] Herzer G 1997 *Handbook of Magnetic Materials* vol 10, ed K H Buschow (Amsterdam: Elsevier) p 415
[32] Ślawska-Waniewska A, Grafoute M and Greneche J M 2006 *J. Phys.: Condens. Matter* **18** 2235
[33] Weller D, Harp G R, Farrow R F C, Cebollada A and Sticht J 1994 *Phys. Rev. Lett.* **72** 2097
[34] Amils X, Nogués J, Suriñach S and Baró M D 1999 *J. Magn. Magn. Mater.* **203** 129
[35] Gleiter H 1989 *Prog. Mater. Sci.* **33** 223
[36] Birringer R 1989 *Mater. Sci. Eng.* A **117** 33
[37] Gallagher K, Johnson F, Kirkpatrick E, Scott J H, Majetich S and McHenry M E 1996 *IEEE Trans. Magn.* **32** 4842
[38] Di L M, Bakker H and De Boer F R 1992 *Physica* B **182** 91